

THE SPECTRAL ENERGY DISTRIBUTION AND EMISSION-LINE PROPERTIES
OF THE NLS1 GALAXY ARAKELIAN 564

P. ROMANO^{1,2}, S. MATHUR¹, T.J. TURNER^{3,4}, S.B. KRAEMER⁵, D.M. CRENSHAW⁶, B.M. PETERSON¹,
R.W. POGGE¹, W.N. BRANDT⁷, I.M. GEORGE^{3,4}, K. HORNE⁸, G.A. KRISS⁹, H. NETZER¹⁰, O.
SHEMMER¹⁰, AND W. WAMSTEKER¹¹

Received 2003 Aug 4; Accepted 2003 Nov 7

ABSTRACT

We present the intrinsic spectral energy distribution (SED) of the Narrow-Line Seyfert 1 galaxy (NLS1) Ark 564, constructed with contemporaneous data obtained during a multi-wavelength, multi-satellite observing campaign in 2000 and 2001. We compare this SED with that of the NLS1 Ton S180 and with those obtained for Broad-Line Seyfert 1s to infer how the relative accretion rates vary among the Seyfert 1 population. Although the peak of the SED is not well constrained, in our parameterization most of the energy of this object is emitted in the 10–100 eV regime, constituting roughly half of the emitted energy in the optical/X-ray ranges. This is consistent with a primary spectral component peaking in the extreme UV/soft X-ray band, and with disk–corona models, hence high accretion rates. Indeed, we estimate that $\dot{m} \approx 1$. We also address the issue of the energy budget in this source by examining the emission lines observed in its spectrum, and we constrain the physical properties of the line-emitting gas through photoionization modeling. The available data suggest that the line-emitting gas is characterized by $\log n \approx 11$ and $\log U \approx 0$, and is stratified around $\log U \approx 0$. Our estimate of the radius of the H β -emitting region $R_{\text{BLR}}^{\text{H}\beta} \approx 10 \pm 2$ lt-days is consistent with the $R_{\text{BLR}}^{\text{H}\beta}$ –luminosity relationships found for Sy1 galaxies, which indicates that the narrowness of the emission lines in this NLS1 is not due to the Broad-Line Region being relatively further away from the central mass than in BLS1s of comparable luminosity. We also find evidence for super-solar metallicity in this NLS1. We show that the emission lines are not good diagnostics for the underlying SEDs and that the absorption line studies offer a far more powerful tool to determine the ionizing continuum of AGNs, especially if comparing the lower- and higher-ionization lines.

Subject headings: galaxies: active – galaxies: individual (Arakelian 564) – galaxies: nuclei – galaxies: Seyfert – galaxies: NLS1 – galaxies: emission lines

1. INTRODUCTION

The population of Seyfert 1 galaxies has a widely used sub-classification into Narrow-Line Seyfert 1 galaxies (NLS1s) and Broad-Line Seyfert 1 galaxies (BLS1s). While this classification appears to make an arbitrary distinction based on the widths of the optical emission lines (NLS1s having $\text{FWHM}(\text{H}\beta) \lesssim 2000 \text{ km s}^{-1}$, Goodrich 1989), this is in fact an extremely useful scheme since the X-ray properties of the two subclasses are systematically different. As a class, NLS1s show rapid and large-amplitude X-ray variability (Boller, Brandt, & Fink 1996, hereafter BBF96; Turner et al. 1999b), with the excess variance (Nandra et al. 1997a) typically an order of magnitude larger than that observed for samples of BLS1s with the same luminosity distribution (Turner et al. 1999b; Leighly 1999a). Analogously, the spectral properties also vary across the Seyfert population with NLS1s showing systematically steeper spectra than those of BLS1s in both the soft and hard X-ray bands (Boller, Brandt, & Fink 1996; Brandt, Mathur, &

Elvis 1997; Turner, George, & Nandra 1998; Leighly 1999b; Vaughan et al. 1999).

One increasingly popular hypothesis to explain the differences in X-ray properties across the Seyfert population is that NLS1s have relatively low masses for the central black hole compared to BLS1s with similar luminosities. Smaller black-hole masses naturally explain both the narrowness of the optical emission lines, which are generated in gas that has relatively small Keplerian velocities, and the extreme X-ray variability, since the primary emission would originate in a smaller region around the central engine (e.g., Laor et al. 1997). Given that NLS1s have comparable luminosity to that of the BLS1s, Pounds, Done, & Osborne (1995) suggested that they must be emitting at higher fractions of their Eddington luminosity, hence higher fractional accretion rates ($\dot{m} = M/\dot{M}_{\text{Edd}}$) are also required. The closer the luminosity is to the Eddington limit (and the lower the black-hole mass), the greater the fraction of the energy emitted by the accretion disk in the soft X-rays

¹ Department of Astronomy, The Ohio State University, 140 West 18th Avenue, Columbus, OH 43210.

² Current address: INAF–Osservatorio Astronomico di Brera, Via E. Bianchi 46, 23807 Merate (LC), Italy; romano@merate.mi.astro.it.

³ Laboratory for High Energy Astrophysics, Code 660, NASA’s Goddard Space Flight Center, Greenbelt, MD 20771.

⁴ Joint Center for Astrophysics, Physics Department, University of Maryland, Baltimore County, 1000 Hilltop Circle, Baltimore, MD 21250.

⁵ Catholic University of America and Laboratory for Astronomy and Solar Physics, NASA’s Goddard Space Flight Center, Code 681, Greenbelt, MD 20771.

⁶ Department of Physics and Astronomy, Georgia State University, Astronomy Offices, One Park Place South SE, Suite 700, Atlanta, GA 30303.

⁷ Department of Astronomy & Astrophysics, The Pennsylvania State University, 525 Davey Laboratory, University Park, PA 16802.

⁸ School of Physics and Astronomy, University of St. Andrews, St. Andrews, KY16 9SS, UK.

⁹ Space Telescope Science Institute, 3700 San Martin Drive, Baltimore, MD 21218.

¹⁰ School of Physics and Astronomy and the Wise Observatory, The Raymond and Beverly Sackler Faculty of Exact Sciences, Tel Aviv University, Tel Aviv 69978, Israel.

¹¹ ESA, P.O. Box 50727, 28080 Madrid, Spain.

(Ross, Fabian, & Mineshige 1992). Thus NLS1s might be expected to show disk components which peak at higher energies than for BLS1s. Pounds, Done, & Osborne (1995) and Maraschi & Haardt (1997) noted that soft photons from the disk may Compton-cool hard X-rays from the corona, and cause the observed steep spectra.

Given the dependence of the peak energy of the disk emission on the accretion rate, the spectral energy distribution (SED) of an active galactic nucleus (AGN) will provide critical information about accretion rates and conditions close to the disk. In particular, examination of the SED of a NLS1, and comparison with that obtained for BLS1s will offer insight into the relative accretion rates across the Seyfert population. However, measuring the SED requires observations taken simultaneously over a long wavelength baseline stretching from infrared to hard X-ray wavelengths, and the determination of the UV/X-ray continuum in AGN is still difficult due to the severe attenuation by even small amounts of Galactic interstellar gas along the line-of-sight. Another complication comes from intrinsic reddening, i.e., reddening associated with the active nucleus itself. Indeed, the steeper UV/blue continua observed in NLS1s (when compared to AGN spectrum composites) can be attributed at least in part to reddening, though the ionization of the absorbing material and its location with respect to the accretion source is still not well determined (Constantin & Shields 2003).

Arakelian 564 (Ark 564, IRAS 22403+2927, MGC +05-53-012) is a bright, nearby NLS1 galaxy, with $z = 0.02467$ and $V = 14.6$ mag (de Vaucouleurs et al. 1991), and a mean 2–10 keV luminosity $L_{2-10\text{ keV}} \approx 2.4 \times 10^{43}$ ergs s^{-1} with flux variations of a factor of a few in a few thousand seconds (Turner et al. 2001, hereafter Paper I). It was the object of an intense multiwavelength monitoring campaign that included simultaneous observations from *ASCA* (2000 June 1 to July 6, Paper I; Pounds et al. 2001; Edelson et al. 2002), *XMM-Newton* (2000 June 17, Vignali et al. 2003), *Chandra* (2000 June 17, Matsumoto, Leighly, & Marshall 2002), *HST* (2000 May 9 to July 8, Collier et al. 2001, Paper II; Crenshaw et al. 2002, Paper IV), *FUSE* (2001 June 29–30, Romano et al. 2002, Paper V), and from many ground-based observatories as part of an AGN Watch¹² project (1998 November to 2001 January, Shemmer et al. 2001, Paper III). Ark 564 has shown a strong associated UV absorber (Crenshaw et al. 1999, Paper II; Paper IV; Paper V). There are indications that it also possesses a warm X-ray absorber, as seen by the narrow absorption lines of O VII and O VIII detected in a *Chandra* spectrum (Matsumoto, Leighly, & Marshall 2002), and that the UV and X-ray absorbers in Arakelian 564 are physically related, possibly identical, and may be spatially extended along the line of sight (Paper V).

In this paper we present a contemporaneous SED of Ark 564, based on the extensive monitoring of 2000. In §2 we describe the observations and data reduction, summarize the main results of the monitoring campaign, and describe the adopted method for reddening correction. In §3 we present the SED of Ark 564. In §4 we constrain the mean physical properties of the line-emitting gas through photoionization modeling. In §5 we discuss some implications of our investigation. Finally, our results are summarized in §6.

2. OBSERVATIONS

2.1. Data Reduction

Table 1 summarizes the log of the observations of Ark 564 used in this study. Column 1 and 2 report the observatory and instrument which obtained the data; Column 3 shows the date in which the data were obtained; Column 4 lists the ranges of energy and wavelength we used for our work; Column 5 lists the total exposure times and the slit size, along with other relevant notes for a particular observation; finally, Column 6 reports the references to the papers where the data were first published. Most of the data have been published already, with the exception of the *XMM* data which will be published in Vignali et al. (2003), therefore here we will only briefly summarize their reduction and analysis, referring the reader to the original papers for further details, and to §2.2 for a summary of the main results.

The *ASCA* data (Paper I) were obtained starting from 2000 Jun 1 (Julian Date 2451697.024) for a total exposure time of ~ 2.98 Ms, and were reduced using standard techniques as described in Nandra et al. (1997a) with the methods and screening criteria utilized by the *Tartarus*¹³ database (Turner et al. 1999b). Data screening yielded an effective exposure time of ~ 1.11 Ms for the SISs and ~ 1.29 Ms for the GISs. The degradation of the low energy response of the SIS detectors was corrected for with the method of Yaqoob et al. (2000)¹⁴, i.e. we parameterized the efficiency loss with a time-dependent absorption ($N_{\text{H}}(\text{SIS0}) = 7.5 \times 10^{20}$ cm^{-2} , $N_{\text{H}}(\text{SIS1}) = 1.05 \times 10^{21}$ cm^{-2} , Paper I).

FUSE observed Ark 564 for 63 ks starting from 2001 June 29 (Paper V). The observations consisted of 24 exposures performed in photon address (time-tag) mode through the $30'' \times 30''$ low-resolution (LWRS) aperture. The data were reduced with *CalFUSE* (version 2.0.5)¹⁵ as a single continuous exposure. As a result of a high-voltage anomaly and data screening, the effective on-source times were 41 ks in Detector 1A, 39 ks in Detector 1B, 58 ks in Detector 2A, and 62 ks in Detector 2B. We discarded from further analysis the SiC1A and SiC1B spectra because of a high-voltage anomaly, and the LiF1B spectrum since it showed wavelength-dependent differences in flux of up to 30–50 % compared to the LiF1A. We rebinned the full spectrum in a linear wavelength scale using 0.6\AA bins (100 pixels, effective resolution of 20 km s^{-1}). Comparison with the flux level of the *HST* spectrum indicates that in June 2001, when the *FUSE* spectrum was obtained, the source was ~ 1.3 times brighter than in May–July 2000, when the *HST* spectrum was obtained. We therefore scaled the *FUSE* fluxes by 0.75 to match the *HST* data. As noted in Paper V, this is not inconsistent with a combination of effects such as flux intercalibration uncertainties and, most importantly, source flux variability.

The *HST* data (Paper II and IV) were obtained with the Space Telescope Imaging Spectrograph (STIS) in 46 visits between 2000 May 9–July 8 (the first five visits were separated by intervals of 5 days, the remaining by 1 day). The spectra were obtained through the $52'' \times 0''.5$ slit and the low-resolution G140L and G230L gratings which yield a spectral resolution of $\sim 1.2\text{\AA}$ and 3.2\AA in the 1150–1730 \AA and 1570–3150 \AA ranges, respectively. The data were reduced using the IDL software

¹² All publicly available data and complete references to published AGN Watch papers can be found at <http://www.astronomy.ohio-state.edu/~agnwatch>.

¹³ <http://tartarus.gsfc.nasa.gov>.

¹⁴ see <http://lheawww.gsfc.nasa.gov/~yaqoob/ccd/nhparam.html>.

¹⁵ See <http://fuse.pha.jhu.edu/analysis/calfuse.html>.

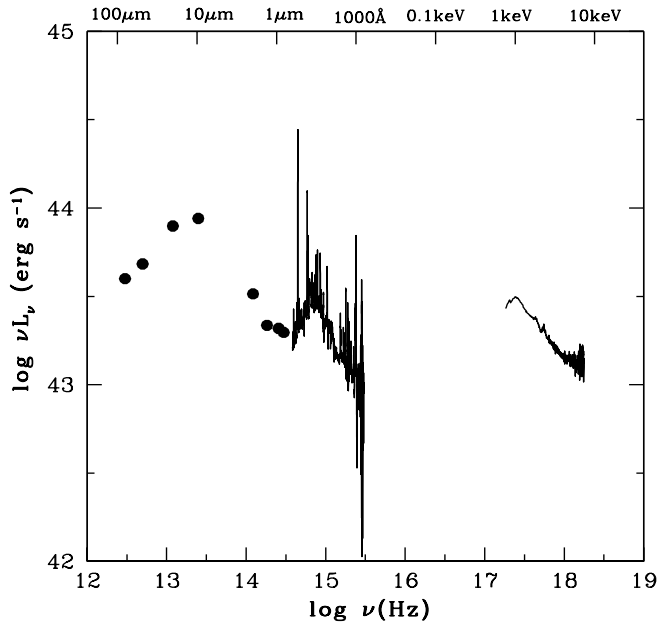


FIG. 1.— Quasi-simultaneous SED of Ark 564 (§2.1). The data have not been corrected for reddening and are in the observed frame.

developed at NASA’s Goddard Space Flight Center for the STIS Instrument Definition Team (Lindler 1998). The spectra have been corrected for small wavelength intercalibration uncertainties following Korista et al. (1995). The uncertainty in the relative wavelength calibration is on the order of 0.6 \AA and 1.7 \AA for the G140L and G230L gratings, respectively. A separate mean spectrum was created for the G140L and G230L grating separately, given the different resolutions.

In the optical we combined two spectra. The first one, which covers the $3170\text{--}4160 \text{ \AA}$ wavelength range with a mean spectral resolution of 0.62 \AA , was obtained in 1980 at Lick Observatory (D. E. Osterbrock 2002, private communication). The second one is the mean of the spectra taken between 1998 Nov to 2001 Jan at the Tel Aviv University Wise Observatory (Paper III, resolution of $\sim 10 \text{ \AA}$). The host galaxy starlight contribution has been estimated by measuring its flux through PSF fitting to field stars in V-band images of the galaxy taken at Wise Observatory, which corresponds to $\sim 40\%$ of the total light at 5200 \AA , i.e. $F_{\text{gal}} = 2.4 \times 10^{-15} \text{ ergs s}^{-1} \text{ cm}^{-2} \text{ \AA}^{-1}$ (Paper III). Given the limited resolution (dominated by a seeing disk of $\sim 2.''5$), it was not possible to separate the components of the host galaxy (bulge and bar) from PSF, hence we subtracted from the mean spectrum a constant host contribution of F_{gal} . No scaling was necessary between the two spectra, in agreement with the low-amplitude variations of the continuum found in Paper II ($\sim 6\%$ over a month-long observation) and III ($\sim 10\%$ during a two-year monitoring). Indeed, there is growing evidence that while NLS1s show very rapid and giant X-ray variability, they show only slow and minor optical variability (O. Shemmer et al 2003, in preparation).

To extend the SED in the IR, we derived four continuum points between ~ 10000 and 24000 \AA from Rodríguez-Ardila et al. (2002a,b), which were obtained on 2000 Oct 11 and 13 with the NASA 3m IRTF telescope and the SPEX spectrome-

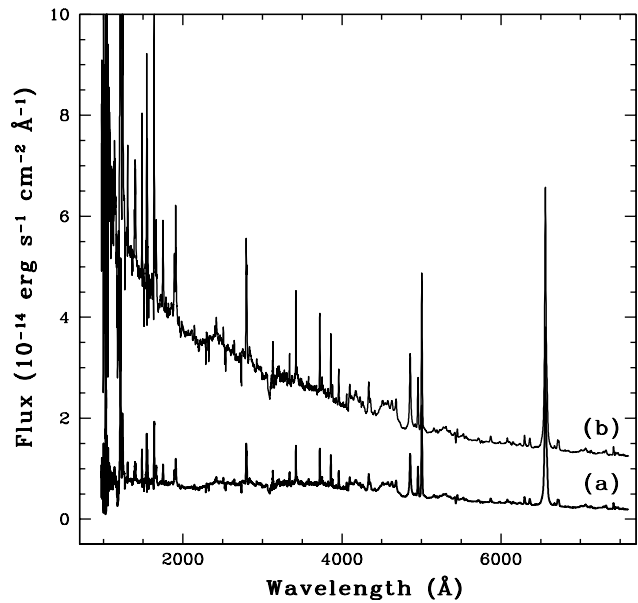


FIG. 2.— (a): FUV/Optical rest-frame spectrum of Ark 564, obtained combining the *FUSE* spectrum (June 2001; $1000\text{--}1175 \text{ \AA}$), the *HST* G140L and G230L mean spectra (May–July 2000; $1175\text{--}3143 \text{ \AA}$), the Lick spectrum (1980; $3170\text{--}4160 \text{ \AA}$), and the Wise mean spectrum (1998 Nov–2001 Jan; $4160\text{--}7790 \text{ \AA}$). The *FUSE* spectrum has been scaled by a factor of 0.75 to match the flux level of the *HST* spectrum; the Wise spectrum has been corrected for the galaxy contribution ($F_{\text{gal}} = 2.4 \times 10^{-15} \text{ ergs s}^{-1} \text{ cm}^{-2} \text{ \AA}^{-1}$; Shemmer et al. 2001). (b): Full spectrum after correction for reddening using a standard Galactic extinction curve with $E(B-V) = 0.03 \text{ mag}$ plus the intrinsic extinction curve that Crenshaw et al. (2002) derive for Ark 564 and $E(B-V) = 0.14 \text{ mag}$. The data have been corrected for redshift ($z = 0.02467$; de Vaucouleurs et al. 1991). The extinction-corrected spectrum (b) has been offset by $1 \times 10^{-14} \text{ ergs s}^{-1} \text{ cm}^{-2} \text{ \AA}^{-1}$ for clarity.

ter. We also retrieved archival *IRAS* flux measurements at 12 , 25 , 60 , and $100 \mu\text{m}$ (Moshir et al. 1990) through the NASA/IPAC Extragalactic Database (NED).

Figure 1 shows the contemporaneous SED of Ark 564 before correction for intervening (and intrinsic, see §2.3) absorption is applied. We note that while the *HST* and Wise spectra are simultaneous (as well as simultaneous with the *ASCA* spectrum), the *FUSE* and Lick spectra were obtained one year later, and 20 years earlier, respectively. The FUV/optical rest-frame spectrum of Ark 564 covering the $1000\text{--}7790 \text{ \AA}$ wavelength region is presented in Figure 2 (labeled as (a)).

2.2. Summary of results from the multi-waveband observations

The continuum fit to the mean *ASCA* spectrum (with a power-law model modified by Galactic absorption, $N_{\text{H}} = 6.4 \times 10^{20} \text{ cm}^{-2}$, Dickey & Lockman 1990) yields a slope $\Gamma = 2.538 \pm 0.005$ (Paper I). The strong excess of emission observed below 2 keV was parameterized as a Gaussian of peak energy $E = 0.57 \pm 0.02 \text{ keV}$ and mean equivalent width (EW) = $110_{-15}^{+11} \text{ eV}$. The soft hump component is also found to be variable in flux on timescales as short as 1 day and in shape on timescales as short as a few days (Paper I). Parameterization of the soft excess as a black-body yields a temperature $T = 1.8 \times 10^6 \text{ K}$ and luminosity $L_{\text{bb}} = 2.48 \times 10^{38} \text{ ergs s}^{-1}$ (Paper I). A strong, ionized ($E \approx 7 \text{ keV}$) Fe $K\alpha$ line is detected, which shows variations in flux and EW on timescales as short as a week (Paper I).

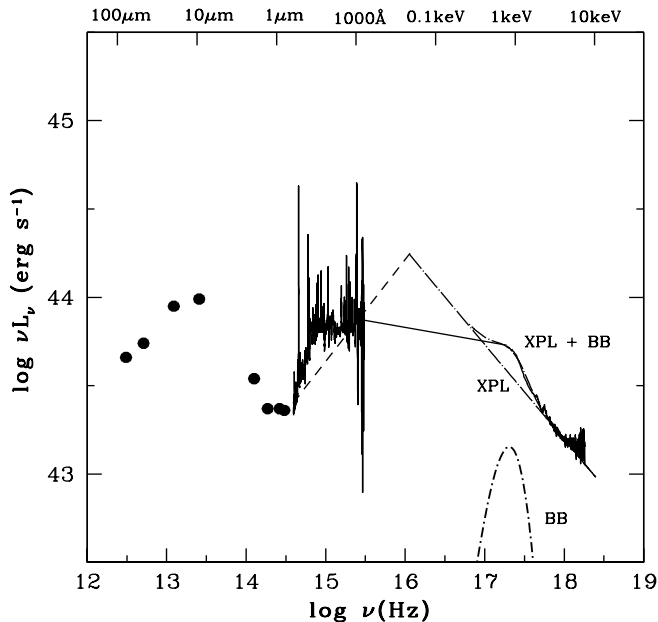


FIG. 3.— Reddening corrected, rest-frame SEDs of Ark 564 (see §3). The optical/FUV data are the spectrum labeled (b) in Figure 2. The X-ray data are drawn from Paper I, while the IR data are from *IRAS* and *IRTF* (§2.1). The short-dashed line shows the power-law fit of the optical/FUV data (spectral index $\alpha = 0.42 \pm 0.01$) extrapolated to higher energies. The long-dash-dot line is the power-law fit to hard X-ray data (XPL, $\alpha_{ASCA} = 1.538 \pm 0.005$, §2.2) extrapolated to lower energies. The short-dash-dot line is the black-body model for the soft X-ray excess (BB, §2.2). The solid line is a more conservative spectral energy distribution (SEDB) that connects the FUV and the soft X-ray data with a simple power law ($\alpha = 1.08$, §3).

The *FUSE* spectrum is dominated by the strong emission in the O VI $\lambda\lambda 1032, 1038$ resonance doublet, and heavily saturated absorption due to Hydrogen Lyman-Werner bands, O VI and C III are observed at velocities near the systemic redshift of Ark 564 (Paper V). The available data suggest that the UV and X-ray absorbers are physically related, possibly identical, and spatially extended along the line of sight, and characterized by total column density and ionization parameter $\log N_{\text{H}} (\text{cm}^{-2}) \approx 21$ and $\log U \approx -1.5$. The absorbing gas is in a state of outflow with respect to the nucleus and carries out a kinetic luminosity about one order of magnitude smaller than the observed radiative luminosity of the source (Paper V).

Variations in the UV continuum flux (1365 Å, Paper II) are well correlated with variations in both the hard (2–10 keV) and soft (0.75–2 keV) X-ray fluxes and with the soft hump flux. No significant lags are detected between the variations in the X-ray and UV bands (Paper I). The variations of the continuum at 3000 Å (Paper II) and at 4900 Å (Paper III) lag behind those at 1365 Å by ~ 1 day and 1.8 days, respectively. These UV/optical delays were interpreted as evidence for a stratified continuum reprocessing region, possibly an accretion disk.

The variations of the Ly α emission line, which lag the variations of the continuum at 1365 Å by 3 days, were used, in conjunction with the line width, to determine the virial mass

of the central black hole, $M \lesssim 8 \times 10^6 M_{\odot}$ (Paper II). This estimate is uncertain due to the low amplitude of the Ly α emission line variations (1%). However, the estimate in Paper II agrees with the one obtained by Pounds et al. (2001) based on a power spectrum analysis of X-ray variability. The black hole mass and 5100 Å luminosity of Ark 564 are consistent with the hypothesis that NLS1s have lower black hole masses and higher accretion rates than BLS1s of comparable luminosity. The low level variability observed in the emission lines is also different from most Seyfert 1 galaxies, which characteristically display variations of 10% on similar timescales.

2.3. Reddening Correction in the Optical/FUV

Given the indications (Paper IV) that strong intrinsic neutral absorption is present in Ark 564 in excess of the Galactic absorption, special care has been taken in correcting the data for reddening. We used a standard Galactic extinction curve with $E(B-V) = 0.03$ mag plus the intrinsic extinction curve that Crenshaw et al. (2002, Paper IV) derive for Ark 564 and $E(B-V) = 0.14$ mag. The *HST* extinction correction was extrapolated linearly into the *FUSE* band, as suggested by Hutchings & Giasson (2001) and Sasseen et al. (2002). The effect of reddening correction in the optical/UV bands is presented in Figure 2, where the observed spectrum in the 1000–7790 Å wavelength region (labeled as (a)) is compared to the absorption-corrected one (labeled as (b)).

3. THE INTRINSIC SED OF ARK 564

Figure 3 shows the Ark 564 data in the IR/X-ray range. A power-law fit of the continuum in the optical/FUV region¹⁶ yields $F_{\lambda} \propto \lambda^{-1.58 \pm 0.01}$, hence spectral index $\alpha = 0.42 \pm 0.01$ (specific flux $f_{\nu} \propto \nu^{-\alpha}$). Extrapolation of this power law in the X-ray regime greatly overpredicts the X-ray flux (dashed line). Analogously, the hard X-ray continuum slope ($\alpha_{ASCA} = \Gamma - 1 = 1.538 \pm 0.005$, §2.2, long-dash-dot line) extrapolated to the lower energies overpredicts the optical/FUV flux, as previously noted by Walter & Fink (1993). Clearly, both the optical/FUV and the X-ray power-laws must break at some energy between the FUV and soft X-ray. With the adopted reddening correction (§2.3), the spectral energy distribution peaks at ~ 50 eV.

Table 2 summarizes some relevant data from the spectral energy distribution derived using the simple parameterization of the combination of an optical/FUV power law with $\alpha = 0.42$ breaking at ~ 50 eV to $\alpha_{ASCA} = 1.538$ (hereon SEDA), as described above, as well as the *IRAS* and *IRTF* data points (§2.1). Column (1) is the rest wavelength/energy, Column (2) and (3) list the observed and reddening corrected values of νL_{ν} , respectively. We estimate that the number of ionizing photons is $Q(\text{SEDA}) \approx 10^{55}$ photons s^{-1} .

We also considered a more conservative spectral energy distribution (the solid line in Figure 3, hereon SEDB) in which the the FUV and the soft X-ray data are connected with a simple power law ($\alpha = 1.08$), i.e. the combination of an optical/FUV power law with $\alpha = 0.42$ breaking at 1000 Å to $\alpha \approx 1$, then again breaking at ≈ 0.8 keV to $\alpha_{ASCA} = 1.538$. The number of ionizing photons for SEDB is $Q(\text{SEDB}) \approx 5 \times 10^{54}$ photons s^{-1} , which

¹⁶ The fit was made to 9 bands: $\lambda = 1005\text{--}1007, 1029.5\text{--}1030.5, 1101\text{--}1107, 1114\text{--}1118, 1155\text{--}1180, 1350\text{--}1380, 1460\text{--}1500, 1620\text{--}1660, \text{ and } 7040\text{--}7050$ Å. The uncertainties are purely statistical. The continuum fit in Paper II was performed only on the *HST* data corrected for Galactic reddening ($E(B-V) = 0.06$ mag) and produced $F_{\lambda} \propto \lambda^{-0.88 \pm 0.01}$; this is comparable to our value for this reddening, $F_{\lambda} \propto \lambda^{-0.73 \pm 0.01}$, since the uncertainties are underestimated in both cases.

is consistent with what Crenshaw et al. (2002) found¹⁷.

4. PHOTOIONIZATION MODELING

In this section, we address the issue of the energy budget of Ark 564 by examining the emission lines observed in its spectrum, and we deduce the mean physical properties of the line-emitting gas, Hydrogen density n and ionization parameter U ($U = Q/4\pi r^2 n c$, r being the distance to the ionizing source and c the speed of light) through photoionization modeling given the assumed spectral energy distributions. We expect a range of ionization to exist throughout the BLR, to accurately describe which multi-zone modeling would be required; however, here we use a single density and ionization parameter modeling to derive the mean BLR properties. For each of the input continua (§4.2), we considered a total hydrogen density of $n = 10^9, 10^{11}, 10^{12}$, and 10^{13} cm^{-3} , and calculated the predicted intensities of the major emission lines, for a range of ionization parameters between $\log U = -4$ and $\log U = 2$. In the case of “table agn” (§4.2), we specified a grid of n and U values. For the other input continua, we normalized the SEDs with respect to the measured X-ray luminosity in the absorption-corrected rest-frame 2–10 keV energy range ($L_{2-10 \text{ keV}} = 2.4 \times 10^{43} \text{ ergs s}^{-1}$; Paper I), and specified the radius of the cloud, thus obtaining U . In the case of SEDA and SEDB, using an observed spectral energy distribution assumes that the gas responsible for the emission lines sees the same ionizing continuum as the observer does; therefore, we expect SEDA and SEDB to yield more realistic predictions of the emitted line spectrum.

4.1. Emission Line Fluxes

The fluxes (relative to $H\beta$) of the most prominent emission lines in the 1150–6817 Å wavelength range have been published in Table 2 of Paper IV; here we report a selection of them in Table 3 (Column (2), relative to $Ly\alpha$). Because of the NLS1 nature of Ark 564, the contribution from the BELR and NELR are strongly blended together and those line ratios include both components. The measured fluxes were corrected for reddening using the continuum reddening curve (Crenshaw et al. 2002), given the similar extinctions for the continuum and emission lines; the errors are propagated in quadrature from the ones listed in Paper IV, and they include photon noise, continuum placement errors, and reddening errors.

Columns (2) and (3) of Table 3 also report the fluxes of C III λ 977 and the O VI $\lambda\lambda$ 1032,1038 doublet, which can help better constrain the value of n and U . These lines were modeled in Paper V, hence both a broad and a narrow component are available (denoted with BEL and NEL, respectively; Columns (2) and (3)). In order to compare with the other line ratios, we needed to account for the different contribution of BELR and NELR gas to $H\beta$, which we estimated as follows. We assumed that the ratio of the narrow component of $H\beta$ and [O III] λ 5007 in NGC 5548, i.e., 0.12 ± 0.01 (Kraemer et al. 1998), can be used for Ark 564; we scaled it to the observed [O III] λ 5007 flux for Ark 564, $F([\text{O III}]\lambda 5007) = (2.4 \pm 0.1) \times 10^{13} \text{ ergs s}^{-1} \text{ cm}^{-2}$ (Paper III), obtaining the NEL ratio $F(H\beta)/F([\text{O III}]\lambda 5007)$ in Ark 564. Thus, we estimated that roughly 75% of the total $H\beta$ flux is from the BEL, and bracketed this value between 50% and 100%, given that the BEL and NEL contributions to C III λ 977 and O VI $\lambda\lambda$ 1032,1038 are the same, and that the total flux is the

absolute upper limit to the BEL flux. We notice that Rodríguez-Ardila, et al. (2000) found that on average, 50% of the flux of the total $H\beta$ is due to emission from the NELR, and that the $F([\text{O III}]\lambda 5007)/F(H\beta)$ emitted in the NELR varies from 1 to 5, which is much lower than our adopted value (~ 8.3). This result is sustained by the analysis of Contini, Rodríguez-Ardila, & Viegas (2003). However, Véron-Cetty, Véron, & Gonçalves (2001) point out that the low $F([\text{O III}]\lambda 5007)/F(H\beta)$ values found by Rodríguez-Ardila, et al. (2000) for NLSy1s are due to the fact that they modeled the broad Balmer component with a Gaussian rather than a Lorentzian. In the analysis of Véron-Cetty, Véron, & Gonçalves (2001) the $F([\text{O III}]\lambda 5007)/F(H\beta)$ ratios span the range measured in BLSys, which makes our use of a value derived from a well-studied BLS1 reasonable. Furthermore, Nagao, Murayama, & Taniguchi (2001) also show that $F([\text{O I}]\lambda 6300)/F([\text{O III}]\lambda 5007)$, $F([\text{O III}]\lambda 4363)/F([\text{O III}]\lambda 5007)$ are indistinguishable in NLS1s and BLS1s. Given this ambiguity, in the following analysis we will note where our assumptions for the deconvolution of O VI $\lambda\lambda$ 1032,1038 and C III λ 977 affect the results.

As a comparison, Column (4) reports the corresponding values for a mean QSO spectrum, which we derived from Baldwin et al. (1995) by applying the reddening correction appropriate for Ark 564; the $H\alpha/Ly\alpha$ ratio is derived from Osterbrock & Pogge (1985). Column (5) lists the BEL fluxes of the Sy1.5 NGC 5548, corrected for NEL contribution and Galactic reddening (Korista & Goad 2000 and references therein). Column (6) lists the FWHM of the lines, as drawn from Papers V, II and III (C III λ 977 and O VI are the model BEL and NEL components, while the others are measured on the whole line profile). All errors are propagated in quadrature. Finally, Column (7) reports the references for Columns (2), (3), and (6). Table 3 shows that Carbon in Ark 564 is at the lower end and Nitrogen at the upper end of the mean QSO distribution, and some interesting differences can be found with respect to the Sy1.5 NGC 5548. Indeed, N V λ 1240 is stronger in Ark 564 by a factor of ~ 2.3 , while C IV λ 1550, C III λ 1909, and Mg II λ 2800 are weaker in Ark 564 by a factor of $\sim 4.4, 2.5$ and 2.8 , respectively.

4.2. Input Continua

We used the code `CLOUDY`¹⁸ (v94.00, Ferland 1996) to predict the intensities of the lines produced by the BEL gas through photoionization modeling. Our choices of input continua for `CLOUDY` are shown in Figure 4. In brief,

1. The `CLOUDY` “table agn” continuum, which is the Mathews & Ferland (1987) continuum modified with a sub-millimeter break at $10 \mu\text{m}$, so that the spectral index is changed from -1 to $-5/2$ for frequencies below the millimeter break.
2. The SEDA input continuum, which was created from points chosen from the spectral energy distribution presented in §3 (the circles in Figure 4), as well as one extrapolated point (the empty square), i.e., where the optical/FUV and X-ray power law extrapolations meet. In particular, in the X-ray, we used continuum points from the power-law fit and added a black body component (the dot-dash line in Figure 3) of temperature

¹⁷ Note that SEDB corresponds to SED2 in Paper V.

¹⁸ <http://www.nublado.org/>.

$T = 1.8 \times 10^6$ K and luminosity $L_{\text{bb}} = 2.48 \times 10^{38}$ ergs s^{-1} (§2.2).

- The more conservative SEDB input continuum, which only uses points from the observed spectral energy distribution (circles only).

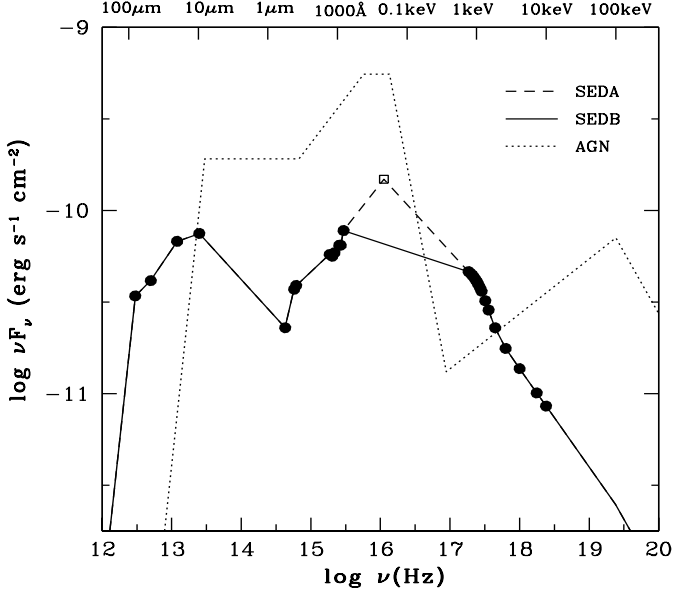


FIG. 4.— Input SEDs for *Cloudy*, normalized to the absorption-corrected rest-frame flux at 2 keV. The dotted line is the “table agn” model in *Cloudy*; the short-dashed line is the SEDA described in §3 (the circles are the observed points, the empty square the extrapolated point); the solid line is the conservative SEDB described in §3.

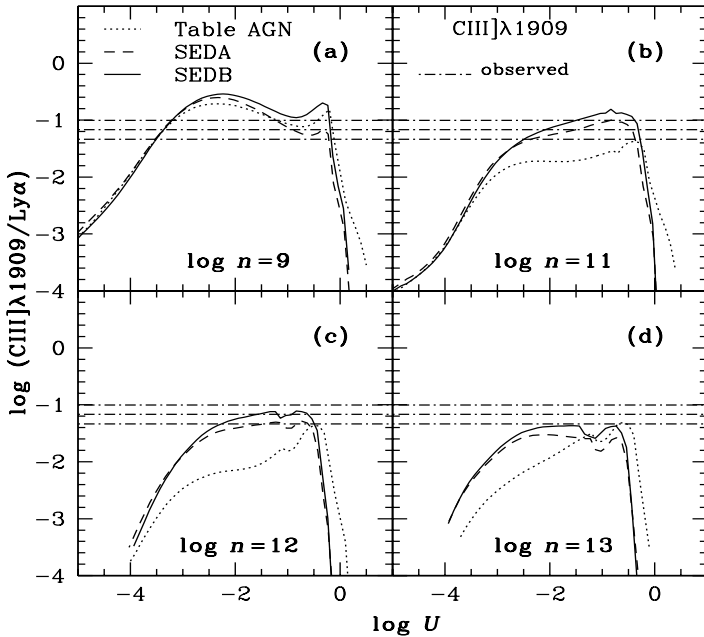


FIG. 5.— Line intensity relative to $\text{Ly}\alpha$ of $\text{C III]}\lambda 1909$ as a function of hydrogen density ($\log n = 9, 11, 12, 13$) and input continuum (“table agn”, SEDA, and SEDB discussed in §4.2). The horizontal dash-dot lines correspond to the observed values and their errors.

4.3. Physical Conditions of the Emission-Line Gas

Figure 5 shows the line intensity of $\text{C III]}\lambda 1909$ relative to $\text{Ly}\alpha$ as a function of hydrogen density ($\log n$ (cm^{-3}) = 9, 11, 12, 13) and input continuum (“table agn”, SEDA, and SEDB discussed in §4.2). The horizontal lines correspond to the observed value of $\text{C III]}\lambda 1909$ and its errors listed in Table 3. Solutions to U (as also shown in Figures 6 and 7) are double valued, but we prefer higher values based on line widths, as discussed below. As expected for a semiforbidden transition, the $\text{C III]}\lambda 1909$ line becomes collisionally suppressed as the density increases, arguing for an upper limit for the density of $\log n \lesssim 12$. Analogously, Figure 6 shows the intensity of $\text{C III}\lambda 977$ and total $\text{N V}\lambda 1240$ which indicate $\log n > 9$. Furthermore, the observed $\text{C III]}\lambda 1909$ implies $\log U \approx -3.3$ or $\log U \approx -0.7$ for $\log n = 9$, both of which are much lower than the values required for O VI , for which we derive $\log U \approx -1.1$ or 0.8^{19} (from a plot analogous to Figure 7b relative to $\log n = 9$), i.e., no consistent result can be found for low densities.

Considering $\log n \approx 11$ as a plausible estimate of the density, we can investigate the value of the ionization parameter. This has been a difficult problem always, because with only optical/UV observations, multiple ionization states of a single element are not observed and so the values of U are highly model dependent. With the multiwavelength, multi-mission observations of Ark 564, we now have observations of both C III (with *FUSE*) and C IV (with *HST*), so we can actually *measure* the ionization parameter. As shown in Figure 7a, the $\text{C III}\lambda 977/\text{C IV}\lambda 1550$ ratio constrains the ionization parameter to $\log U = [-2.88, -0.22]^{20}$. Studies of reverberation mapping have shown that the BLR is stratified (Peterson & Wandel 1999), and so a single value of U cannot possibly correspond to the entire BLR, but the range of U determined above must be the dominant range of U where C IV emission is produced. The higher ionization lines, e.g. $\text{O VI}\lambda\lambda 1032, 1038$ and $\text{He II}\lambda 1640$ are likely to be produced closer in with higher ionization parameter. Indeed, as shown in Figure 7b, and Figure 6d, somewhat higher values of U are preferred for O VI ($\log U = [-1.52, -1.36]$ or $\log U = [0.61, 0.87]^{21}$) and N V ($\log U = [-1.43, 0.4]$).

Figure 7c shows the $\text{C IV}\lambda 1550$ intensity ratio and implies that either $\log U = [-2.94, -2.66]$ or $\log U = [0.18, 0.34]$. Figure 7d shows the intensity ratio $\text{C IV}\lambda 1240/\text{N V}\lambda 1550$, for which we derive $\log U = [0.07, 0.39]$. The comparison with the BLS1 NGC 5548 shows that N V is stronger in Ark 564 by a factor of ~ 2.3 , while C IV is weaker in Ark 564 by a factor of ~ 4.4 (§4.1 and Table 3). Hence, the observed $\text{C IV}/\text{N V}$ ratio may be roughly one order of magnitude smaller in Ark 564, and the observed limits in Figure 7d probably reflect an overabundance of N (or C depletion).

To discriminate between the low- U ($\log U \approx -1.5$) and high- U ($\log U \approx 0$) solutions, we derive the distance of the BELR gas from $R_{\text{BELR}} = (Q/4\pi cnU)^{1/2} \approx 1.63 \times 10^{16} (Q_{55}/U)^{1/2} n_{11}^{-1/2}$ cm, where $Q_{55} = Q/10^{55}$, assuming the above values of U and n , and the photon luminosity Q from §3. For $\log n = 11$ and $\log U \approx -1.5$, the inferred distance of the BELR is $R_{\text{BELR}}^{\text{SEDA}} = 9.2 \times 10^{16}$ cm for $Q(\text{SEDA})$, and $R_{\text{BELR}}^{\text{SEDB}} = 6.5 \times 10^{16}$ cm for $Q(\text{SEDB})$. For $\log n = 11$ and $\log U \approx 0$, $R_{\text{BELR}}^{\text{SEDA}} = 1.63 \times 10^{16}$ cm and $R_{\text{BELR}}^{\text{SEDB}} = 1.15 \times 10^{16}$ cm. For a central mass of $M =$

¹⁹ We find $\log U \approx -0.9$ or 0.8 if we do not deconvolve BEL and NEL.

²⁰ $\log U = [-3.07, -0.36]$ if we do not deconvolve BEL and NEL.

²¹ $\log U = [-1.44, -1.23]$ or $\log U = [0.64, 0.79]$ if we do not deconvolve BEL and NEL.

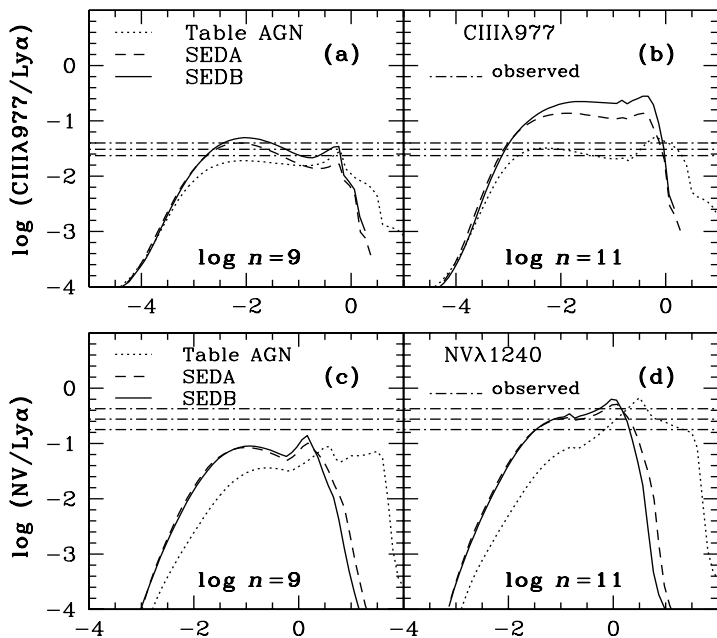


FIG. 6.— Same as Figure 5 for C III λ 977 (top) and N V λ 1240 (bottom) for $\log n = 9$ and 11.

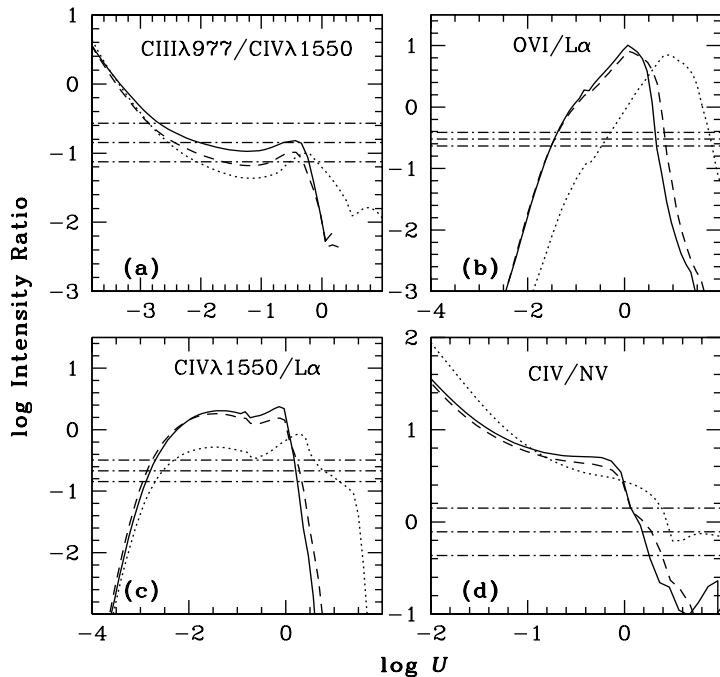


FIG. 7.— Line intensity ratios of C III λ 977 / C IV λ 1550 (a), O VI / $\text{Ly}\alpha$ (b), C IV λ 1550 / $\text{Ly}\alpha$ (c), and C IV λ 1550 / N V λ 1240 (d), as function of input continuum (same line notations as in Figure 5). For all cases, $\log n = 11$.

$8 \times 10^6 M_{\odot}$, the expected velocity dispersion (Peterson et al. 2000) is $V = (GM/R_{\text{BLR}}f)^{0.5}$, with $f = 3/\sqrt{2}$. This corresponds

to 740–880 km s⁻¹ for the low- U solutions and 1750–2090 km s⁻¹ for the high- U solutions. Column (6) of Table 3 shows that $\text{FWHM}(\text{C IV}) = 1934$ km s⁻¹, $\text{FWHM}(\text{C III}) = 1920$ km s⁻¹, and $\text{FWHM}(\text{N V}) = 2809$ km s⁻¹. Therefore, the comparison with the observed FWHMs favors the high- U solutions. Finally, Table 3 shows that the FWHM of O VI is larger than that of N V, which is larger than that of C IV, again consistent with the stratified BLR model.

5. DISCUSSION

A non-simultaneous optical, UV and X-ray spectral energy distribution of Ark 564 was presented by Comastri et al. (2001) who found that it peaks in the soft-X-ray band. Here we present a spectral energy distribution which is obtained from contemporaneous data covering almost 5 decades in energy²². Simultaneity is particularly important for NLS1s, since, as a class, they are extremely variable in time, although Ark 564 has shown only weak variability in the optical/UV bands (Paper II-III).

We report some relevant data from the spectral energy distribution in Table 2. These were derived using the simple parameterization of the combination of an optical/FUV power law with spectral index $\alpha = 0.42$ breaking at ~ 50 eV to $\alpha_{\text{ASCA}} = 1.538$ (SEDA in Figure 3), as well as the *IRAS* and *IRTF* data points (§2.1). A more conservative spectral energy distribution, instead, connects the FUV and the soft X-ray data with a simple power law ($\alpha = 1.08$, the solid line in Figure 3), and is a combination of an optical/FUV power law with $\alpha = 0.42$ breaking at 1000 Å to $\alpha = 1.081$, then again breaking at ≈ 0.8 keV to $\alpha_{\text{ASCA}} = 1.538$ (SEDB in Figure 3). The ambiguity in the shape of the spectral energy distribution in the 900 Å–0.8 keV region is rather unfortunate, since a considerable portion of the energy of Ark 564 might be output in this range. Previous *ROSAT* (Brandt et al. 1994) and *BeppoSAX* (Comastri et al. 2001) data showed a flattening of the soft excess toward the lowest X-ray energies available, and the *XMM* spectrum obtained during the monitoring campaign of 2000 shows a definite curvature in the soft excess (Vignali et al. 2003).

An interesting issue is how Ark 564 compares to other NLS1 galaxies and with BLS1 in terms of its broad-band properties, as they can be quantified by spectral indices. Table 4 reports the intrinsic spectral indices calculated between different wavelength bands for Ark 564 and, as a comparison, the corresponding values for the NLS1 Ton S180 and BLS1s. These show that while the inter-band properties of Ton S180 are not significantly different from the ones observed in BLS1s (Turner et al. 2002), this may not be the case for Ark 564. Table 4 indicates that the two NLS1s have steeper X-ray slopes than BLS1s, Ark 564 more so than Ton S180 ($\alpha_x = 1.57$ and 1.44, respectively, compared to 0.91 for BLS1s), which is consistent with the general characteristics of NLS1s. The optical/X-ray spectral index (α_{ox}), on the other hand, is lower in Ark 564 than in BLS1s and Ton S180 with $\alpha_{\text{ox}} = 1.11$ for Ark 564²³, 1.52 for Ton S180. This reflects the fact that Ark 564 is relatively more X-ray bright, or that the optical continuum is suppressed, compared to other AGNs. The other indices also reflect the X-ray brightness of Ark 564 when compared to BLS1s. We cannot exclude the possibility that intrinsic reddening in excess of the

²² The Lick spectrum, which was obtained in 1980 is merely used to fill in a small gap in the optical data, and the 2001 *FUSE* spectrum shows a continuum slope consistent with the one obtained from the *HST* spectrum. This latter fact suggests that, although the flux level changed between 2000 and 2001, the overall shape of the optical/FUV spectral energy distribution did not change.

²³ The observed α_{ox} is 0.94 in Ark 564.

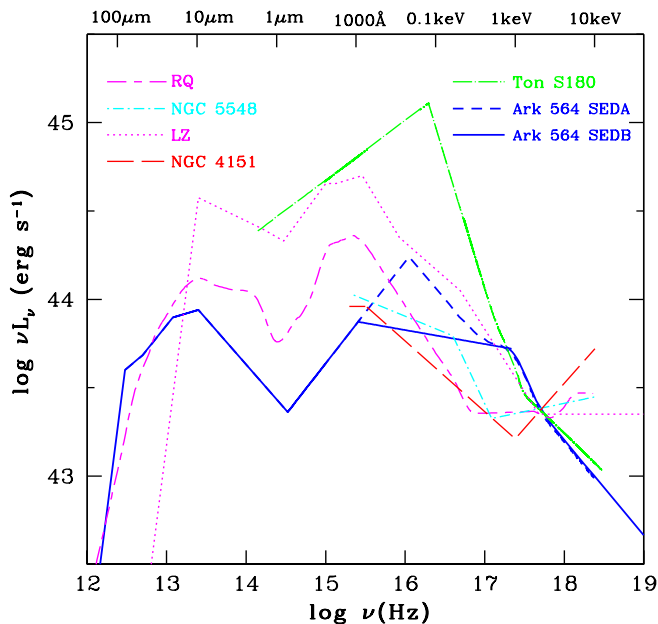


FIG. 8.— Comparison of the SEDs of Ark 564 with the mean SED for radio-quiet quasars (RQ; Elvis et al. 1994) and LZ (Laor et al. 1997; Zheng et al. 1997), one Seyfert 1 galaxy (NGC 4151, Kraemer et al. 2000), one Seyfert 1.5 galaxy (NGC 5548, Kraemer et al. 1998, and the NLS1 Ton S180 (Turner et al. 2002). [A color version of this plot is available in the electronic edition of the Journal.]

one considered here may be present that could be suppressing the optical, but we argue that it would require the continuum to be more reddened than the emission lines (e.g. He II $\lambda 1640/\lambda 4686$ ratio; Paper IV) show. If these differences, however, are not due to intrinsic reddening, then they represent a true difference in the energy balance of this NLS1 and that the X-ray emission is therefore consistent with the predictions of the slim disk models, indicating high accretion rates.

We estimated the luminosity in different energy bands using our parameterizations of the spectral energy distribution described above (SEDA and SEDB). Though with a $\sim 20\%$ systematic error in the 0.3–0.6 keV band flux (C. Vignali 2003, private communication), the *XMM* spectrum provides a way to extend the energy range below the ~ 0.8 keV limit of the *ASCA* spectrum. Therefore, we also estimated the luminosity for the best-fit model to this spectrum. Table 5 reports these luminosities, and indicates that more energy is emitted in the 10–100 eV band than in any other decade, constituting roughly half of the emitted energy in the opt/X-ray ranges. This implies that the primary spectral component peaks in the extreme UV–soft X-ray band and this is generally consistent with disk-corona models (Haardt & Maraschi 1991). The integrated luminosity between 10^{-5} and 10 keV gives a lower limit on the bolometric luminosity of $L_{\text{bol}} \gtrsim 10^{45}$ ergs s^{-1} .

Growing evidence has been gathered that NLS1s are super-Eddington accretors. Collin & Huré (2001) and Collin et al. (2002) studied accretion rates in a sample of AGNs using the Kaspi et al. (2000) relationship, and found that not only half of their sample accretes close to or above the Eddington rate,

but also that the largest Eddington ratios are found in NLS1s. Indeed, they showed that NLS1s are at the extreme of a well-defined sequence relating the Eddington ratio to the line widths. Furthermore, Wang & Netzer (2003) show that a model of extreme slim disk (which is responsible for the soft X-ray excess, or hump, seen in most NLS1s) and a hot corona (contributing to the hard X-ray emission) can also naturally explain the X-ray spectral variability characteristics observed in Ark 564 such as simultaneous variations of the soft hump and the hard X-ray without a significant time lag (Turner et al. 2001). Through a comparison of the X-ray variability of Ark 564 and the BLS1 NGC 3516, Pounds et al. (2001) estimate that the mass of the central black hole in Ark 564 is $\sim 10^7 M_{\odot}$, implying an accretion rate in the range $\dot{m} \approx 0.2$ –1. With a bolometric luminosity in the order of 10^{45} ergs s^{-1} and an Eddington luminosity $L_{\text{Edd}} \approx 10^{45}$ ergs s^{-1} , we also infer that $\dot{m} \approx 1$. Wang & Netzer (2003) also provide a means of estimating the black hole mass (if the accretion is super-critical) which is independent on the accretion rate itself. For Ark 564, we obtain $M \approx 2 \times 10^6 M_{\odot}$, which is within a factor of a few from the Collier et al. (2001) estimate.

Figure 8 compares the SED of Ark 564 with the mean SED for radio-quiet quasars (Elvis et al. 1994), the LZ SED (Laor et al. 1997; Zheng et al. 1997), the Seyfert 1.5 galaxies NGC 5548 (Kraemer et al. 1998) and NGC 4151 (Kraemer et al. 2000), and the NLS1 Ton S180 (Turner et al. 2002). There are significant differences in the intrinsic shape of the SED across the AGN population (see, also, Turner et al. 2002), the most evident being the energy of the peak and the presence (or lack of) of the big blue bump (BBB), the signature of the emission from the accretion disk. The radial dependence of the temperature for an optically thick, geometrically thin accretion disk (Shakura & Sunyaev 1973) is, $T(R) \sim 6.3 \times 10^5 (\dot{m})^{1/4} M_8^{-1/4} (R/R_S)^{-3/4}$ K (Peterson et al. 2000), where M_8 is the mass in units of $10^8 M_{\odot}$, R is the radius, and R_S is the Schwarzschild radius. For Ark 564, using $\dot{m} \approx 1$, as we derived above, and $M \approx 8 \times 10^6 M_{\odot}$ (Paper II), the peak temperature is ~ 125 eV; this is within a factor of 3 from the peak of our less conservative parameterization, SEDA (defined extrapolating the optical power-law continuum to meet the extrapolation of the X-ray power law) which peaks at 50 eV. The true SED probably peaks somewhere between these two values. For comparison, the NLS1s RE J1034+396 (Puchnarewicz et al. 2001) and Ton S180 (Turner et al. 2002) peak at ≈ 250 eV and $\lesssim 100$ eV, respectively. Therefore, even among the NLS1s, differences in the shape of the SED are observed. However, in none of these NLS1s there is an indication of the presence of optical/UV BBB, and a strong soft X-ray excess is seen, instead. In this light, Ark 564, is also consistent with the paradigm that the accretion disk is so hot in NLS1s that the BBB is shifted in the EUV–soft X-rays.

We also note that Ark 564 is rather FIR bright (with respect to the optical), compared to the sample of radio-quiet quasars and the LZ sample, as can be seen in Figure 9, where the SEDs have been normalized to match their optical/UV slope (as opposed to the 2 keV flux in Figure 8). Indeed, if we use the definition of the IR flux as a function of the *IRAS* fluxes given by Sanders & Mirabel (1996)²⁴, we obtain that $L(8-1000 \mu\text{m}) \approx 10^{11} L_{\odot}$, which makes Ark 564 a luminous IR galaxy. The shape of the IR/optical SED of Ark 564 also resembles the shapes observed in the *IRAS* Bright Galaxy Survey (see Figure 2 in Sanders & Mirabel 1996, for intermediate values of f_{60}). Using SEDA, we

²⁴ $F(8-1000 \mu\text{m}) = 1.8 \times 10^{-14} \{13.48f_{12} + 5.16f_{25} + 2.58f_{60} + f_{100}\}$ W m^{-2} , where f_{12} , f_{25} , f_{60} , and f_{100} are the *IRAS* flux densities in Jy at 12, 25, 60 and 100 μm .

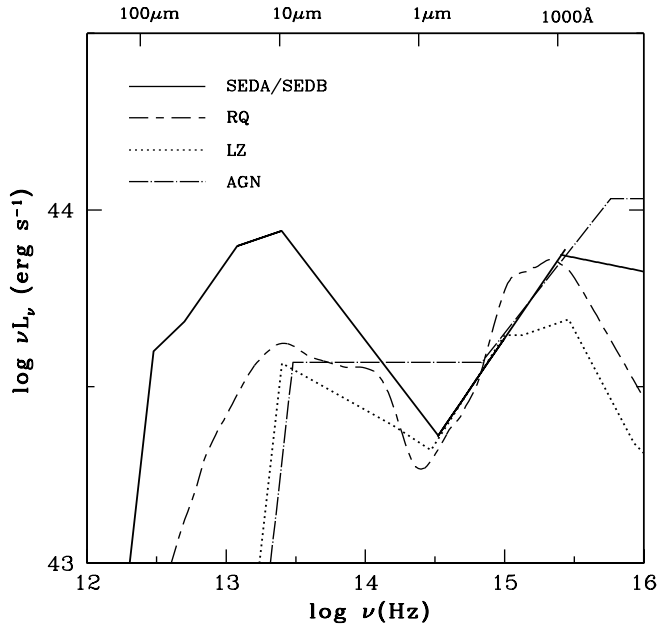


FIG. 9.— Comparison of the Ark 564 SED with the mean SED for radio-quiet quasars (RQ; Elvis et al. 1994), LZ (Laor et al. 1997; Zheng et al. 1997), and the “table agn” model in Cloudy (AGN). The SEDs are normalized so that they match in the optical/UV part.

estimate that the FIR luminosity is $L_{\text{FIR}} \approx 1.3 \times 10^{44}$ ergs s^{-1} , i.e., $\sim 10\%$ of the total luminosity and $\sim 20\%$ of the combined optical/UV/X-ray luminosity. Crenshaw et al. (2002) noted that the associated warm UV absorber is lukewarm and dusty. The IR emission observed in this object could then be thermal emission from the dust grains embedded in the absorber as they are heated by the strong UV/EUV continuum. Given the IR brightness in this object and in many NLS1s (Moran, Halpern, & Helfand 1996), it is not unlikely that a contribution might be coming from the host galaxy, in the form of a nuclear starburst (Mathur 2000). Crenshaw et al. (2002), however, did not detect any extended emission in the two-dimensional STIS spectral images that could be due to a nuclear starburst. We compared the *FUSE* spectrum, which was taken through a much larger aperture, and hence is more likely to show stellar absorption features, with a *FUSE* ‘template’ spectrum of the starburst galaxy NGC 7496; using the constraints from the Ly γ –C III] λ 977 profiles, we obtained a rough upper limit of the starburst contribution at 1000Å of 50%. A further constraint on the IR starburst contribution would probably come from detection and measurements of the 3.3–3.4 μ m PAH emission features, which have been found in starburst galaxies, luminous IR galaxies, and obscured AGNs (Moorwood 1986; Imanishi 2002), and which have been successfully detected in the NLS1 NGC 4051 (Rodríguez-Ardila & Viegas 2003).

Using our SEDA and SEDB as inputs to Cloudy we predicted the intensity of the strongest lines in the FUV/UV spectrum and compared them with the observed values in order to constrain the physical parameters of the line-emitting gas, namely, the density and ionization parameter. Figure 6 and 7 show that SEDA and SEDB, because of their strong EUV to soft X-ray flux, for a given observed line ratio predict values of ionization parameter which are lower than those with stan-

dard AGN continuum. From C III] λ 1909, C III λ 977, and N V λ 1240, we infer that $\log n \approx 11$. Two classes of solutions for U are consistent with this density value, one with low U values ($\log U \approx -1.5$) and one with high U values ($\log U \approx 0$). We discarded the low- U class (§4.3) on the basis that the predicted widths of the lines, derived from the velocity dispersion $V = (GM/R_{\text{BLR}}f)^{0.5}$, of 740–880 km s^{-1} are too small with respect to the observed ones (≈ 2000 km s^{-1} ; Paper II). As expected, we find that the BLR is stratified around $\log U \approx 0$, with higher ionization lines originating from regions with higher U .

Column (6) of Table 3 shows that $\text{FWHM}(\text{Ly}\alpha) = 2114$ km s^{-1} , $\text{FWHM}(\text{N V}) = 2809$ km s^{-1} , and $\text{FWHM}(\text{C IV}) = 1934$ km s^{-1} , which indicate that the radii of the Ly α , N V, and C IV broad-line emitting regions are $R_{\text{BLR}}^{\text{Ly}\alpha} \approx 4.3$ lt-days, $R_{\text{BLR}}^{\text{N V}} \approx 2.5$ lt-days, and $R_{\text{BLR}}^{\text{C IV}} \approx 5.2$ lt-days. Using the findings of previous monitoring programs on Seyfert 1s (Netzer & Peterson 1997), we can estimate the size of the H β -emitting region from $R_{\text{BLR}}^{\text{Ly}\alpha} \approx 0.5R_{\text{BLR}}^{\text{H}\beta}$, and $R_{\text{BLR}}^{\text{N V}} \approx 0.2R_{\text{BLR}}^{\text{H}\beta}$. For NGC 5548, furthermore, $R_{\text{BLR}}^{\text{C IV}} \approx 0.5R_{\text{BLR}}^{\text{H}\beta}$ (Peterson 1993). We can conclude that $R_{\text{BLR}}^{\text{H}\beta} \approx 10 \pm 2$ lt-days, which is consistent with the $R_{\text{BLR}}^{\text{H}\beta}$ –luminosity relationships of Kaspi et al. (2000) and Peterson et al. (2000), when we assume a luminosity $\lambda L_{\lambda}(5100 \text{ \AA}) \approx 3.2 \times 10^{43}$ ergs s^{-1} (Table 2). This indicates that the BLR radius of this NLS1 is consistent with the distribution of BLR radius in BLS1s, and that the narrowness of the emission lines is not due to the BLR being relatively further away from the central mass than in BLS1s of comparable luminosity.

Table 3 shows that some interesting differences in line ratios can be found with respect to the Sy1.5 NGC 5548. Indeed, N V λ 1240 is stronger in Ark 564 by a factor of ~ 2.3 , while C IV λ 1550, C III] λ 1909, and Mg II λ 2800 are weaker in Ark 564 by a factor of ~ 4.4 , 2.5 and 2.8, respectively. While all line ratios in Ark 564 are statistically consistent with the ones measured for a mean QSO (given the large uncertainties on our measurements), Carbon lines are at the lower end and Nitrogen at the upper end of the QSO distribution, confirming this trend for weak Carbon and strong Nitrogen in Ark 564. Furthermore, C III] λ 977 would indicate that $-3.13 < \log U < -0.05$ (Figure 6), and for this range, the observed N V/C IV ratio is larger than the model predictions by a factor of ~ 8 . This may imply super-solar metallicity in this NLS1 as suggested by Mathur (2000) and is consistent with the finding of Shemmer & Netzer (2002) that NLS1s have higher metallicities than BL AGNs for a given luminosity.

An interesting question is how sensitive the emission lines are to the true shape of the ionizing continuum. Given the difficulty related to deblending the BEL and NEL components of the lines and consequent large errors on the observed line ratios, the present emission line data do not allow us to discriminate between SEDA and SEDB. These SEDs differ in the range 1000Å–750 eV (corresponding to the gap in the data between the *FUSE* and *ASCA* spectra), with the maximum difference at around 50 eV. This difference should show the most for the high ionization lines of C IV, N V and O VI. However, the predicted strength of their *emission* lines is very similar for the two SEDs, for a wide range of ionization parameters of interest (Figures 6 and 7). Perhaps, this is the reason why the emission line spectra of most AGNs look so very similar, over a wide range of luminosities. This demonstrates how unsuitable emission lines are as diagnostics for the underlying SEDs.

The absorption lines, on the other hand, are sensitive to the

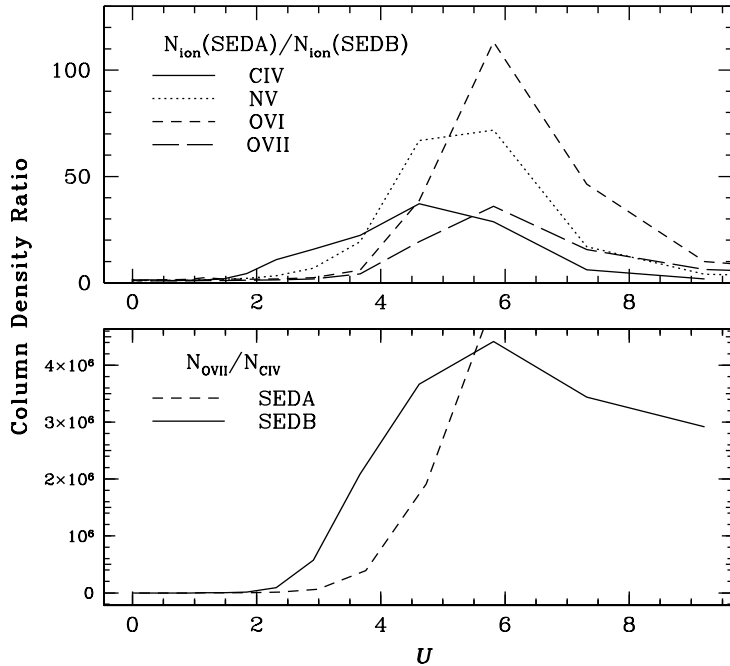


FIG. 10.— Top panel shows the ratio of the column densities relative to SEDA and SEDB as a function of U for C IV, N V, O VI, and O VII. Bottom panel shows the ratio of the column densities of O VII to C IV as a function of U for solar abundances, for SEDA and SEDB.

input SED (Mathur et al. 1994). Column densities of different ions can be inferred from the fractional abundances f_{ion} , the total column density N_{H} , and the assumed abundances N_{X} , $N_{\text{ion}} = N_{\text{H}} N_{\text{X}} N_{\text{ion}}$, through photoionization calculations (assuming an SED). Figure 10 (Top) shows the fractional column densities for the same ion calculated with the different SEDs [$N_{\text{CIV}}(\text{SEDA}) / N_{\text{CIV}}(\text{SEDB})$, $N_{\text{NV}}(\text{SEDA}) / N_{\text{NV}}(\text{SEDB})$, $N_{\text{OVI}}(\text{SEDA}) / N_{\text{OVI}}(\text{SEDB})$, and $N_{\text{OVII}}(\text{SEDA}) / N_{\text{OVII}}(\text{SEDB})$], and illustrates how the predicted column densities of high ionization lines differ, with O VI showing the largest variations, with over two orders of magnitude difference. Figure 10 (Bottom) compares the column density for O VII and C IV calculated with the same SED and solar abundances [$N_{\text{OVII}}(\text{SEDA}) / N_{\text{CIV}}(\text{SEDA})$ and $N_{\text{OVII}}(\text{SEDB}) / N_{\text{CIV}}(\text{SEDB})$], which turn out to be good diagnostics even at lower ionization parameters. Thus, in principle, absorption line studies offer a far more powerful tool to determine the ionizing continuum of AGNs, compared to the emission lines. This also underscores the power of multiwavelength observations, as the maximum discriminator comes from comparing the lower- and higher-ionization lines.

6. SUMMARY

We presented the intrinsic spectral energy distribution of Ark 564, constructed with quasi-simultaneous data obtained during 2000 and 2001. We compared this SED with that of Ton S180 and with those obtained for Broad-Line Seyfert 1s to infer how the relative accretion rates vary among the Seyfert 1 population. The peak of the SED is not well constrained; however, in our parameterization most of the energy of this object is emitted in the 10–100 eV regime, and constitutes roughly half of the emitted energy in the optical/X-ray ranges. This is consistent with a primary spectral component peaking in the soft X-ray band, therefore with the predictions of the slim disk models, hence high accretion rates. Indeed, we estimate that $\dot{m} \approx 1$.

We constrained the mean physical conditions in the BELR of this AGN, by examining the emission lines observed in its spectrum, and deduced the physical properties of the line-emitting gas through photoionization modeling. We concluded that the line-emitting gas is characterized by $\log n \approx 11$ and $\log U \approx 0$, and is stratified around $\log U \approx 0$. Our estimate of the radius of the $\text{H}\beta$ emitting region $R_{\text{BLR}}^{\text{H}\beta} \approx 10 \pm 2$ lt-days, is consistent with the $R_{\text{BLR}}^{\text{H}\beta}$ -luminosity relationships of Kaspi et al. (2000) and Peterson et al. (2000). This indicates that the narrowness of the emission lines is not due to the BLR being relatively further away from the central mass than in BLS1s of comparable luminosity. We also find evidence for super-solar metallicity in this NLS1, based on the low C IV/N V observed line ratio. While the emission lines turn out to be unsuitable as diagnostics for the underlying SEDs, we showed that absorption line studies offer a far more powerful tool to determine the ionizing continuum of AGNs, especially if comparing the lower- and higher-ionization lines. This underlines the power of multiwavelength observations.

We thank C. Vignali for providing us with the *XMM* spectrum ahead of publication and the anonymous referee for suggestions that improved the paper. P.R. and S.M. acknowledge support through NASA grant NAG5-10320 (*FUSE*), and the Italian MIUR. T. J. T. and W. N. B. acknowledge support through NASA LTSA grants NAG5-7385 and NAG5-13035, respectively. We also acknowledge support from HST-GO-08265.01-A from the Space Science Telescope Institute, which is operated by the Association of Universities for Research in Astronomy, Inc., under NASA contract NSS5-226555. This research has made use of the NASA/IPAC Extragalactic Database (NED) which is operated by the Jet Propulsion Laboratory, California Institute of Technology, under contract with the National Aeronautics and Space Administration.

REFERENCES

- Alexander, T., Sturm, E., Lutz, D., Sternberg, A., Netzer, H., & Genzel, R. 1999, *ApJ*, 512, 204
 Arav, N., Kaastra, J., Steenbrugge, K., Brinkman, B., Edelson, R., Korista, K. T., & de Kool, M. 2003, *ApJ*, 590, 174
 Baldwin, J., Ferland, G., Korista, K., & Verner, D. 1995, *ApJ*, 455, L119
 Boller, Th., Brandt, W. N., & Fink, H. 1996, *A&A*, 305, 53
 Brandt, W. N., Fabian, A. C., Nandra, K., Reynolds, C. S., & Brinkmann, W. 1994, *MNRAS*, 271, 958
 Brandt, W. N., Mathur, S., & Elvis, M. 1997, *MNRAS*, 285, L25
 Brotherton, M. S., Green, R. F., Kriss, G. A., Oegerle, W., Kaiser, M. E., Zheng, W., & Hutchings, J. B. 2002, *ApJ*, 565, 800
 Cardelli, J. A., Clayton, G. C., & Mathis, J. S. 1989, *ApJ*, 345, 245
 Cheng, F. H., Gaskell, C. M., Koratkar, A. P. 1991, *ApJ*, 370, 487
 Collier, S. J., et al. 2001, *ApJ*, 561, 146 (Paper II)
 Collin, S. & Huré, J.-M. 2001, *A&A*, 372, 50
 Collin, S., Boisson, C., Mouchet, M., Dumont, A.-M., Coupé, S., Porquet, D., & Rokaki, E. 2002, *A&A*, 388, 771
 Comastri, A., et al. 2001, *A&A*, 365, 400
 Constantin, A. & Shields, J. C. 2003, *PASP*, 115, 592
 Contini, M., Rodríguez-Ardila, A., & Viegas, S. M. 2003, *A&A*, 408, 101
 Crenshaw, D. M., Kraemer, S. B., Bogges, A., Maran, S. P., Mushotzky, R. F., & Wu, C. 1999, *ApJ*, 516, 750
 Crenshaw, D. M., et al. 2002, *ApJ*, 566, 187 (Paper IV)
 de Vaucouleurs, G., de Vaucouleurs, A., Corwin, H. G., Buta, R. J., Paturel, G., & Fouque, P. 1991, *S&T*, 82, 621
 Czerny, B. & Elvis, M. 1987, *ApJ*, 321, 305
 Dickey, J. M., & Lockman, F. M. 1990, *ARA&A*, 28, 215
 Edelson, R., et al. 2002, *ApJ*, 568, 610

- Elvis, M., et al. 1994, *ApJS*, 95, 1
- Ferland, G. J. 1996, *Hazy*, a brief introduction to Cloudy 94.00, Univ. Kentucky Dept. Phys. Astron. Int. Rep.
- Ferrarese, L., Pogge, R. W., Peterson, B. M., Merritt, D., Wandel, A., & Joseph, C. L. 2001, *ApJ*, 555, L79
- Goodrich, R. W. 1989, *ApJ*, 342, 234
- Grube, D., Beuermann, K., Thomas, H.-C., Mannheim, K., & Fink, H. H. 1998, *A&A*, 330, 25
- Haardt, F., & Maraschi, L., 1991, *ApJ*, 380, 51
- Huchra, J. P., Vogeley, M. S., & Geller, M. J. 1999, *ApJS*, 121, 287
- Hutchings, J. B. & Giasson, J. 2001, *PASP*, 113, 1209
- Imanishi, M. 2002, *ApJ*, 569, 44
- Kaspi, S. et al. 1996, *ApJ*, 470, 336
- Kaspi, S., Smith, P. S., Netzer, H., Maoz, D., Jannuzi, B. T., & Giveon, U. 2000, *ApJ*, 533, 631
- Korista, K., et al. 1995, *ApJS*, 97, 285
- Korista, K. T. & Goad, M. R. 2000, *ApJ*, 536, 284
- Kraemer, S. B., Crenshaw, D. M., Filippenko, A. V., & Peterson, B. M. 1998, *ApJ*, 499, 719
- Kraemer, S. B., Crenshaw, D. M., Hutchings, J. B., Gull, T. R., Kaiser, M. E., Nelson, C. H., & Weistrop, D. 2000, *ApJ*, 531, 278
- Laor, A., Fiore, F., Elvis, M., Wilkes, B. J., & McDowell, J. C. 1997, *ApJ*, 477, 93
- Lawrence, A., Elvis, M., Wilkes, B. J., McHardy, I., Brandt, N. 1997, *MNRAS* 285, 879
- Leighly, K. M. 1999a, *ApJS*, 125, 297
- Leighly, K. M. 1999b, *ApJS*, 125, 317
- Lindler, D. 1998, *CALSTIS Reference Guide (CALSTIS Version 5.1)*
- Maraschi, L., Haardt, F. 1997, in *IAU Colloq. 163, Accretion Phenomena and related Outflows*, ed. D. Wickramasinghe, L. Ferrario, & G. Bicknell, Pub. of the ASP Press
- Mathews, W. G. & Ferland, G. J. 1987, *ApJ*, 323, 456
- Mathur, S. 2000, *MNRAS*, 314, L17
- Mathur, S., Wilkes, B., Elvis, M., & Fiore, F. 1994, *ApJ*, 434, 493
- Matsumoto, C., Leighly, K. M., & Marshall, H. L. 2002, *X-ray Spectroscopy of AGN with Chandra and XMM-Newton*, 263
- Moorwood, A. F. M. 1986, *A&A*, 166, 4
- Moran, E. C., Halpern, J. P., & Helfand, D. J. 1996, *ApJS*, 106, 341
- Moshir, M. & et al. 1990, *IRAS Faint Source Catalogue*, version 2.0 (1990), 0
- Nagao, T., Murayama, T., & Taniguchi, Y. 2001, *ApJ*, 546, 744
- Nandra, K., George, I. M., Mushotzky, R. F., Turner, T. J., & Yaqoob, T. 1997a, *ApJ*, 477, 602
- Nandra, K., George, I. M., Mushotzky, R. F., Turner, T. J., & Yaqoob, T. 1997b, *ApJ*, 477, 602
- Netzer, H. & Peterson, B. M. 1997, *ASSL Vol. 218: Astronomical Time Series*, 85
- Osterbrock, D. E. & Pogge, R. W. 1985, *ApJ*, 297, 166
- Peterson, B. M. 1993, *PASP*, 105, 247
- Peterson, B. M. & Wandel, A. 1999, *ApJ*, 521, L95
- Peterson, B. M. et al. 2000, *ApJ*, 542, 161
- Pounds, K. A., Done, C., & Osborne, J. P. 1995, *MNRAS*, 277, L5
- Pounds, K. A., Edelson, R., Markowicz, A., & Vaughan, S. 2001, *ApJ*, 550, L15
- Puchnarewicz, E. M., Mason, K. O., Romero-Colmenero, E., Carrera, F. J., Hasinger, G., McMahon, R., & Mittaz, J. P. D., Page, M. J., Carballo, R. 1996, *MNRAS*, 281, 1243
- Puchnarewicz, E. M., Mason, K. O., Siemiginowska, A., Fruscione, A., Comastri, A., Fiore, F., & Cagnoni, I. 2001, *ApJ*, 550, 644
- Rodríguez-Ardila, A., Binette, L., Pastoriza, M. G., & Donzelli, C. J. 2000, *ApJ*, 538, 581
- Rodríguez-Ardila, A., Viegas, S. M., Pastoriza, M. G., & Prato, L. 2002, *ApJ*, 565, 140
- Rodríguez-Ardila, A., Viegas, S. M., Pastoriza, M. G., & Prato, L. 2002, *ApJ*, 579, 214
- Rodríguez-Ardila, A. & Viegas, S. M. 2003, *MNRAS*, 340, L33
- Romano, P., Mathur, S., Pogge, R. W., & Peterson, B. M., & Kuraszkiewicz, J. 2002, *ApJ*, 578, 64 (Paper V)
- Ross, R., Fabian, A. C., & Mineshige, S. 1992, *MNRAS*, 258, 189
- Sanders, D. B. & Mirabel, I. F. 1996, *ARA&A*, 34, 749
- Sasseen, T. P., Hurwitz, M., Dixon, W. V., & Airieau, S. 2002, *ApJ*, 566, 267
- Schlegel, D. J., Finkbeiner, D. P., & Davis, M. 1998, *ApJ*, 500, 525
- Shakura, N. I., & Sunyaev, R. A. 1973, *A&A*, 24, 337
- Shemmer, O., et al. 2001, *ApJ*, 561, 162 (Paper III)
- Shemmer, O. & Netzer, H. 2002, *ApJ*, 567, L19
- Turner, T. J., George, I. M., & Nandra, K. 1998, *ApJ*, 508, 648
- Turner, T. J., et al. 1999a, *ApJ*, 510, 178
- Turner, T. J., et al. 1999b, in *Proceedings of the 19th Texas Symposium on Relativistic Astrophysics and Cosmology*, ed. J. Paul, T. Montmerle, & E. Aubourg (Saclay: CEA), E441
- Turner, T. J., Romano, P., George, I. M., Edelson, R., Collier, S. J., Mathur, S., & Peterson, B. M. 2001, *ApJ*, 561, 131 (Paper I)
- Turner, T. J., et al. 2002, *ApJ*, 568, 120
- Vaughan, S., Reeves, J., Warwick, R., & Edelson, R. 1999, *MNRAS*, 309, 113
- Véron-Cetty, M.-P., Véron, P., & Gonçalves, A. C. 2001, *A&A*, 372, 730
- Vignali C., Brandt W. N., Boller Th., Fabian A. C., Vaughan S., 2003, *MNRAS*, submitted 05/26/03
- Walter, R. & Fink, H. H. 1993, *A&A*, 274, 105
- Wang, J.-M. & Netzer, H. 2003, *A&A*, 398, 927
- Yaqoob, T., et al. 2000, *ASCA GOF Calibration Memo*, ASCA-CAL-00-06-01, v1.0
- Zamorani, G., et al. 1981, *ApJ*, 245, 357
- Zheng, W., Kriss, G. A., Telfer, R. C., Grimes, J. P., & Davidsen, A. F. 1997, *ApJ*, 475, 469

TABLE 1
OBSERVING LOG FOR ARAKELIAN 564

Observatory (1)	Instrument (2)	UT Dates (3)	Wavelength/Energy ^a (4)	Notes (5)	References (6)
<i>ASCA</i>		2000 Jun 1–Jul 6	0.75–9.76 keV	2.98 Ms, continuous ^b	1
<i>XMM-Newton</i>		2000 Jun 17	0.3–8 keV		2
<i>FUSE</i>		2001 Jun 29–30	1000–1175 Å	63 ks; 30''x 30''(LWRS)	3
<i>HST</i>	STIS/G140L	2000 May 9–Jul 8	1175–1711 Å	554304 s; 52''x 0''5	4,5
<i>HST</i>	STIS/G230L	2000 May 9–Jul 8	1711–3143 Å	24216 s; 52''x 0''5	4,5
Lick		1980	3170–4160 Å		6
Wise	FOSC	1998 Nov–2001 Jan	4160–7790 Å		7
<i>IRTF</i>	SPEX	2000 Oct 11, 13	8200–24000 Å ^c	~ 30 min, 15''x 0''8	8
<i>IRAS</i>			12, 25, 60, 100 μm		9

^aObserved-frame wavelength/energy bands utilized.

^bExcept for gaps due to Earth occultation and passage of the spacecraft through the SAA.

^cOnly few continuum points were used for this work.

References. — (1) Turner et al. 2001. (2) Vignali et al. 2003. (3) Romano et al. 2002. (4) Collier et al. 2001. (5) Crenshaw et al. 2002. (6) D. E. Osterbrock 2002, private communication; (7) Shemmer et al. 2001. (8) Rodríguez-Ardila et al. 2002b and references therein. (9) Moshir et al. 1990.

TABLE 2
DATA FROM THE SPECTRAL ENERGY DISTRIBUTION

Rest Wavelength /Energy (1)	νL_ν (Observed) ($\times 10^{43}$ ergs s $^{-1}$) (2)	νL_ν (Intrinsic, SEDA) ($\times 10^{43}$ ergs s $^{-1}$) (3)
97.59 μm^{a}	3.98	4.57
58.56 μm^{a}	4.82	5.50
24.40 μm^{a}	7.91	8.91
11.71 μm^{a}	8.73	9.77
2.4 μm^{b}	3.3	3.5
1.6 μm^{b}	2.2	2.4
1.14 μm^{b}	2.1	2.4
1 μm^{c}	2.045	2.165
9850, \AA^{b}	2.0	2.3
7000 \AA	1.851	2.660
5500 \AA	1.73	3.057
5100 \AA	1.694	3.193
3000 \AA	1.461	4.338
2500 \AA	1.388	4.819
1000 \AA	1.075	8.178
0.046 keV $^{\text{d}}$...	17.5
0.25 keV $^{\text{d}}$...	7.195
0.78 keV	2.895	5.240
1 keV	3.046	4.668
2 keV	2.060	2.419
10 keV	0.942	0.970

Note. — The intrinsic optical/UV/X-ray data are from the reddening-corrected, rest-frame SEDA (§3). SEDB is SEDA with the exclusion of the point at ~ 50 eV. We adopt $H_0 = 75$ km s $^{-1}$ Mpc $^{-1}$, $q_0 = 0.5$.

^aIRAS data points (§2.1).

^bIRTF data points (§2.1).

^cExtrapolated value from the optical/FUV power law (spectral index $\alpha = 0.42 \pm 0.01$, §3).

^dExtrapolated value from the ASCA power law ($\alpha_{\text{ASCA}} = 1.538 \pm 0.005$, §2.2), peak of SEDA (§3).

TABLE 3
ARAKELIAN 564 EMISSION-LINE CHARACTERISTICS

Line	F/F(Ly α) BEL+NEL ^a	F/F(Ly α) BEL ^a	F/F(Ly α) QSO ^b	F/F(Ly α) NGC5548 ^c	FWHM (km s ⁻¹) ^d	References
(1)	(2)	(3)	(4)	(5)	(6)	(7)
C III λ 977	0.053 \pm 0.017	0.031 \pm 0.015	4000,1100	1,2
O VI λ 1032	0.284 \pm 0.032	0.200 \pm 0.052	...	0.036	4000,1100	1,2
O VI λ 1038	0.141 \pm 0.048	0.100 \pm 0.026	...	0.018	4000,1100	1,2
O VI λ 1032,1038	0.425 \pm 0.141	0.300 \pm 0.076	0.1–0.3 ^e	0.054	4000,1100	1,2
L α λ 1216	1.00	1.00	1.00	1.00	2114	3,4
N V λ 1240	0.275 \pm 0.118	...	0.09–0.26	0.119	2809	3,4
C IV λ 1550	0.215 \pm 0.087	...	0.28–0.42	0.937	1934	3,4
He II λ 1640	0.101 \pm 0.040	...	0.06–0.13 ^f	0.143 ^f	1195,1831	3,4
O III] λ 1663	0.038 \pm 0.015	3,4
C III] λ 1909	0.068 \pm 0.026 ^g	...	0.09–0.19 ^h	0.171 ^g	1920	3,4
Mg II λ 2800	0.066 \pm 0.008	...	0.06–0.13	0.188	1659	3,5
H β λ 4861	0.063 \pm 0.019	...	0.02–0.05	...	700	3
H α λ 6563	0.240 \pm 0.080	...	0.05–0.09 ⁱ	3

^aReddening-corrected flux relative to Ly α derived from Crenshaw et al. (2002). The lines are corrected using $E(B-V) = 0.14 \pm 0.04$ mag and Ark 564 reddening curve from Crenshaw et al. (2002) plus $E(B-V) = 0.03$ mag and Galactic curve (§2.3).

^bData from the mean observed QSO spectrum in Baldwin et al. (1995) and references therein, corrected for the reddening appropriate for Ark 564.

^cBEL fluxes, corrected for NEL contribution and Galactic reddening of the Sy1.5 NGC 5548; derived from Korista & Goad (2000) and references therein. The O VI line ratios are derived from the BEL values in Brotherton et al. (2002), then corrected for Galactic reddening ($E(B-V) = 0.03$ mag, and extinction law of Cardelli, Clayton, & Mathis 1989).

^dModel FWHM of C III λ 977 and O VI relative to BEL and NEL components (Paper V), separately; the others are measured on the whole line profile (Paper II). The He II values are relative to the G140L and G230L mean spectrum, respectively (Paper II).

^eTotal O VI+Ly β flux. This compares with 0.434 ± 0.141 for Ark 564.

^fTotal He II+O III] λ 1666 flux. This compares with 0.139 ± 0.043 for Ark 564.

^gTotal C III] λ 1909+Si III] λ 1892 flux.

^hTotal C III] λ 1909+Si III] λ 1892+Al III λ 1990 flux.

ⁱBased on the range of values of H α /H β (3.97–6.64) from the NLS1 sample of Osterbrock & Pogge (1985).

References. — (1) This work. (2) Paper V. (3) Paper IV. (4) Paper II. (5) Paper III.

TABLE 4
SPECTRAL INDICES

Index (1)	Definition (2)	Ark 564 ^a (3)	Ton S180 ^a (4)	BLSy1 (5)	References (6)
$\alpha_{100\mu\text{m}-12\mu\text{m}}$	$-1.086 \log(F_{12\mu\text{m}}/F_{100\mu\text{m}})$	0.64			
$\alpha_{12\mu\text{m}-2.4\mu\text{m}}$	$-1.431 \log(F_{2.4\mu\text{m}}/F_{12\mu\text{m}})$	1.64			
$\alpha_{2.4\mu\text{m}-1.6\mu\text{m}}$	$-5.679 \log(F_{1.6\mu\text{m}}/F_{2.4\mu\text{m}})$	1.94			
$\alpha_{1.6\mu\text{m}-1\mu\text{m}}$	$-4.900 \log(F_{1\mu\text{m}}/F_{1.6\mu\text{m}})$	1.18 ^b			
$\alpha_{12\mu\text{m}-1\mu\text{m}}$	$-0.927 \log(F_{1\mu\text{m}}/F_{12\mu\text{m}})$	1.60 ^b			
$\alpha_{3000-1000}$ (α_{uv})	$-2.096 \log(F_{1000}/F_{3000})$	0.42	0.66	1.25	1
$\alpha_{FUSE-ASCA}$ ^c		1.08			1
$\alpha_{5500-0.25\text{keV}}$	$-0.489 \log(F_{0.25\text{keV}}/F_{5500})$	0.82 ^b	1.12	0.73	2
$\alpha_{5500-1\text{keV}}$ ($\alpha_{\text{ox-hard}}$)	$-0.378 \log(F_{1\text{keV}}/F_{5500})$	0.93	1.38	1.13	3
$\alpha_{1\mu\text{m}-2\text{keV}}$ (α_{ix})	$-0.312 \log(F_{2\text{keV}}/F_{1\mu\text{m}})$	1.01 ^b	1.35	1.14-2.16	4
$\alpha_{2500-2\text{keV}}$ (α_{ox})	$-0.384 \log(F_{2\text{keV}}/F_{2500})$	1.11	1.52	$1.46^{+0.05}_{-0.07}$, 1.21 ± 0.02	5,6
α_{x}	$-1.431 \log(F_{10\text{keV}}/F_{2\text{keV}})$	1.57	1.44	0.91	7

Note. — For spectral indices relative to the Ark 564 *IRAS* points we used the reddening-corrected, redshift-corrected fluxes and wavelengths.

^aIntrinsic, i.e. reddening-corrected, redshift-corrected (SEDA).

^bBased on extrapolated value (§3, Figure 3).

^cSimple power law connecting the high energy end of the *FUSE* spectrum and the low energy end of the *ASCA* spectrum (§3, Figure 3).

References. — (1) Cheng, Gaskell & Koratkar 1991; index in the 2200-1200 Å band, based on the BLS1 subsample. (2) Turner et al. 1999a. (3) Grupe et al. 1998. (4) Lawrence et al. 1997. (5) Zamorani et al. 1981. (6) Puchnarewicz et al. 1996. (7) Nandra et al. 1997b.

TABLE 5
LUMINOSITIES

Energy Range (keV) (1)	L (Observed) ($\times 10^{44}$ ergs s^{-1}) (2)	L (SEDA) ^a ($\times 10^{44}$ ergs s^{-1}) (3)	L (SEDB) ^a ($\times 10^{44}$ ergs s^{-1}) (4)	L (XMM) ^a ($\times 10^{44}$ ergs s^{-1}) (5)
$10^{-5}-10^{-4}$...	2.1192	2.1192	2.1192
$10^{-4}-10^{-3}$...	1.8108	1.8108	1.8108
$10^{-3}-0.01$...	1.2464	1.2464	1.2464
0.01-0.1	...	3.5175	2.2589	4.1430
0.1-1	0.2201	1.6314	1.8080	2.7716
1-10	0.4086	0.4485	0.4485	0.5285
$10^{-5}-10$...	10.7738	9.6918	12.6202

^aReddening-corrected, rest-frame luminosities.

Note. — The SEDA luminosities have been calculated using power-law parameterization of the SED with the spectral indices reported in Table 4. The SEDB luminosities refer to the more conservative parameterization described in §3 (Figure 3). The XMM luminosities make use of the *XMM* spectrum in the 0.05–10 keV band.